Neuroscience Research 98 (2015) 50–58

Contents lists available at ScienceDirect

Neuroscience Research

journal homepage: www.elsevier.com/locate/neures

Connectivity analysis of normal and mild cognitive impairment patients based on FDG and PiB-PET images

Seong-Jin Son[a], Jonghoon Kim[a], Jongbum Seo[b], Jong-min Lee[c], Hyunjin Park[d,*], the ADNI[1]

[a] Department of Electronic Electrical and Computer Engineering, Sungkyunkwan University, Republic of Korea
[b] Department of Biomedical Engineering, Yonsei University, Republic of Korea
[c] Department of Biomedical Engineering, Hanyang University, Republic of Korea
[d] School of Electronic and Electrical Engineering, Sungkyunkwan University, Republic of Korea

ARTICLE INFO

Article history:
Received 4 December 2014
Received in revised form 2 April 2015
Accepted 8 April 2015
Available online 17 April 2015

Keywords:
Connectivity analysis
FDG-PET
PiB-PET
Mild cognitive impairment

ABSTRACT

Connectivity analysis allows researchers to explore interregional correlations, and thus is well suited for analysis of complex networks such as the brain. We applied whole brain connectivity analysis to assess the progression of Alzheimer's disease (AD). To detect early AD progression, we focused on distinguishing between normal control (NC) subjects and subjects with mild cognitive impairment (MCI). Fludeoxyglucose (FDG) and Pittsburgh compound B (PiB)-positron emission tomography (PET) were acquired for 75 participants. A graph network was implemented using correlation matrices. Correlation matrices of FDG and PiB-PET were combined into one matrix using a novel method. Group-wise differences between NC and MCI patients were assessed using clustering coefficients, characteristic path lengths, and betweenness centrality using various correlation matrices. Using connectivity analysis, this study identified important regions differentially affected by AD progression.

1. Introduction

Alzheimer's disease (AD) is the most common form of dementia and has worldwide implications (Berchtold and Cotman, 1998; Brookmeyer, 1998; Hebert and Scherr, 2003). Many AD patients transition from a cognitively normal status to an intermediate stage called mild cognitive impairment (MCI), before finally converting to AD. There is no generally-accepted cure for far-progressed AD, and thus early detection of AD is important. Various imaging modalities, including magnetic resonance imaging (MRI), single photon emission tomography (SPECT), and positron emission tomography (PET) have been successfully applied to assess the progression of AD in patients (Greicius et al., 2004; Matsuda, 2007; Fripp et al., 2008; Frisoni et al., 2010; Mosconi et al., 2010a). The usage of PET has led to many discoveries in AD research as well (Klunk et al., 2004; Foster et al., 2007; Koivunen et al., 2008; Fripp et al., 2008; Mosconi et al., 2010a; Bohnen and Djang, 2012; Hatashita and Yamasaki, 2013). PET imaging provides contrast information derived from local radiotracer activity. PET imaging using fludeoxyglucose (FDG) reflects local metabolism by region glucose uptake, which has been shown to be effective at distinguishing normal subjects from patients with AD (Foster et al., 2007; Mosconi et al., 2010a; Bohnen and Djang, 2012; Ishii, 2013). Pittsburgh compound B (PiB) is a radiotracer that binds to a well-established biomarker of AD known as beta-amyloid (Klunk et al., 2004; Koivunen et al., 2008; Fripp et al., 2008; Hatashita and Yamasaki, 2013). PET imaging using PiB (PiB-PET) provides contrast information based on local deposition of beta-amyloid, which has shown a high correlation with the progression of AD in patients (Klunk et al., 2004; Koivunen et al., 2008; Hatashita and Yamasaki, 2013). Many brain regions show decreased FDG-PET activity for AD patients compared to normal while the same regions show increased PiB-PET activity (Hatashita and Yamasaki, 2013; Klunk et al., 2004). A multi-modal PET study should exhibit this anti-proportional behavior of FDG and PiB PET.

Raw data from imaging modalities cannot be used directly for extracting relevant information for AD research. Imaging data are processed using various algorithms implemented in software packages for proper research (Friston and Holmes, 1994; Jenkinson et al., 2012). Many of these image-processing algorithms are intended to identify regions that reflect group-wise differences. Another type of algorithm, known as connectivity analysis, focuses on how activities in one region correlate with activities in another region of a complex network (Anwander et al., 2007; He et al., 2007; Bullmore and Sporns, 2009). Connectivity analysis allows observation of the

* Corresponding author. Tel.: +82 31 299 4956; fax: +82 31 290 5819.
E-mail address: hyunjinp@skku.edu (H. Park).

[1] Data used in this article were obtained from the Alzheimer's Disease Neuroimaging Initiative (ADNI) database.

http://dx.doi.org/10.1016/j.neures.2015.04.002
0168-0102/

whole brain as a complex, connected network. Well-established theories and tools borrowed from network graphs can be applied to quantify the connectivity of any given brain (Bullmore and Sporns, 2009; He and Evans, 2010; Watts and Strogatz, 1998). Connectivity in our study refers to functional connectivity whose information is derived from functional imaging modalities such as fMRI or PET. The functional connectivity is primarily a statistical concept measured via correlation between distinct regions, which many studies adopted (Zalesky et al., 2012). It is different from structural connectivity where physical neuronal fibers connect two distinct regions. If two regions share a similar signal pattern, be it from blood-oxygen-level-dependent (BOLD) signal or some other relevant signal, the strength of functional connectivity is assumed to be high. Many studies successfully applied functional connectivity analysis to resting state fMRI and FDG-PET and the brain networks identified were large consistent with known brain circuitries (He and Evans, 2010; Seo et al., 2013; Wang et al., 2013; Zalesky et al., 2012). Some studies went further an adopted a morphological feature, cortical thickness, to compute connectivity (He et al., 2007; Wee et al., 2013; Wheeler et al., 2015). If two regions share a similar pattern of cortical thickness, the connectivity was assumed to be high. In the same vein, we applied functional connectivity analysis to patterns of amyloid deposition for PiB-PET. In this study, connectivity derived from PET reflects correlation between patterns of regional cerebral metabolism (FDG) or amyloid deposition (PiB). Connectivity analysis typically involves a matrix whose elements reflect some degree of correlation between two regions of interest (ROIs). The matrix, referred to as the correlation matrix, contains correlation values that are derived from underlying imaging modalities. More and more studies have adopted multi-modal approaches, thereby a single brain is described in two or more modalities. In such scenarios, more than two correlation matrices need to be combined properly for further analysis. Combing correlation matrices requires careful attention, because the matrices are derived from different modalities.

The focus of this study is to assess information regarding MCI in patients showing AD progression. We attempt to distinguish MCI from normal cognitive aging in an effort to detect AD progression early on. Unlike many studies that utilize various methods of MRI to investigate AD, we utilized PET imaging. We obtained FDG-PET and PiB-PET imaging from the Alzheimer's Disease Neuroimaging Initiative (ADNI), an extensive research database on the topic (Carrillo et al., 2012). For our purposes, connectivity analysis was applied to PET images of normal control (NC) and MCI patients. Each imaging modality resulted in a separate correlation matrix, which we later combined using pseudo-logical operations. Group-wise differences (i.e., differences between MCI and NC subjects) were assessed using clustering coefficients, characteristic path lengths, and betweenness centrality. The goals of this study are (1) to apply connectivity analysis to two types of PET imaging, FDG-PET and PiB-PET, and (2) to combine the results of the connectivity analyses of both types of PET imaging in a novel way. As a brief preview of the findings, we were able to combine different correlation matrices and to replicate important known ROIs for AD progression.

2. Materials and methods

2.1. Subjects and PET images

We collected two types of PET imaging, PiB and FDG imaging, from the ADNI database (Carrillo et al., 2012). For FDG-PET, the following imaging parameters were used on a Siemens scanner. Image matrix = 128 × 128; number of slices = 63; pixel resolution = 2 mm × 2 mm; slice thickness = 2.4 mm; radiopharmaceutical = 18F-FDG, reconstruction method = iterative. For PiB-PET, the following imaging parameters were used on a Siemens scanner. Image matrix = 128 × 128; number of slices = 63; pixel resolution = 2 mm × 2 mm; slice thickness = 2.4 mm; radiopharmaceutical = 11C-PiB, reconstruction method = iterative. In patients, MCI can be associated with non-AD type dementias such as vascular or Lewy body dementia, which we excluded in this study (Hansen and Samuel, 1997; Braak et al., 1999; Lee et al., 2009). We focused on the type of MCI that is an early stage of AD known as "MCI due to AD." Seventy-five patients were divided into NC ($n = 20$) and MCI ($n = 20$) sub-groups for the FDG group, and NC ($n = 15$) and MCI ($n = 20$) sub-groups for the PiB group. Patients in the NC group had global clinical dementia rating (CDR) scores of 0 and mini-mental state examination (MMSE) scores between 27 and 30. Patients in the MCI group had global CDR scores of 0.5 and MMSE scores between 20 and 26 (Folstein et al., 1975; Morris, 1993). Details regarding the patient groups, including age and sex ratios, are provided in Table 1. There were no significant differences (p-value > 0.05) between the groups in age or sex ratio.

Table 1
Demographic information for NC and MCI groups. Mean and standard deviation values are reported.

PET tracer	Information	NC ($n = 20$)	MCI ($n = 20$)	p-Value
FDG	Gender (M:F)	12:8	14:7	0.6673
	Age	76.34 (6.41)	78.49 (7.19)	0.3245
	MMSE score	30 (0)	22.9 (1.74)	<0.001
	CDR score	0 (0)	0.5 (0)	0
PET tracer	Information	NC ($n = 15$)	MCI ($n = 20$)	p-Value
PiB	Gender (M:F)	9:6	12:8	1
	Age	77.78 (6.23)	76.07 (6.68)	0.4445
	MMSE score	29 (1)	23.65 (1.87)	<0.001
	CDR score	0 (0)	0.5 (0)	0

2.2. Image pre-processing and ROIs

The PET images in the ADNI database were standardized from different systems using a system of pre-processing steps. First, each extracted frame of PET is co-registered to the first extracted frame of the raw image file (frame acquired at 30–35 min post-injection). The base frame image and the five co-registered frames (or all the co-registered frames for quantitative studies) are recombined into a co-registered dynamic image set. Second, the co-registered dynamic image set is averaged to create a single 30-minute PET image, which averages six 5-min frames (or the last six frames for quantitative studies). Third, each subject's co-registered, averaged image from their baseline PET scan is then reoriented into a standard 160 × 160 × 96 grid, having 1.5-mm cubic voxels. This image grid is oriented in such a way that the anterior–posterior axis of the subject is parallel to the anterior–posterior commissure (AC-PC) line. Fourth, each image obtained from the third step is filtered with a scanner-specific filter function to produce images of a uniform isotropic resolution of 8-mm full width half maximum (FWHM), the approximate resolution of the lowest resolution scanners used in the ADNI database. The standardized uptake value (SUV) of PET is normalized by the mean SUV of the cerebellar region.

Connectivity analysis requires specifying ROIs in order for any correlations among them to be investigated. ROIs can be specified manually or by automatic methods. We used an automatic method to propagate ROIs from a pre-defined atlas onto the standard space. A well-known atlas with 90 labeled ROIs is available as a result of previous research (Tzourio-Mazoyer et al., 2002). We applied an image registration software based on C/C++ to register the atlas with the standard space of PET using mutual information cost function and affine geometric transform (Meyer et al., 1997). Once the

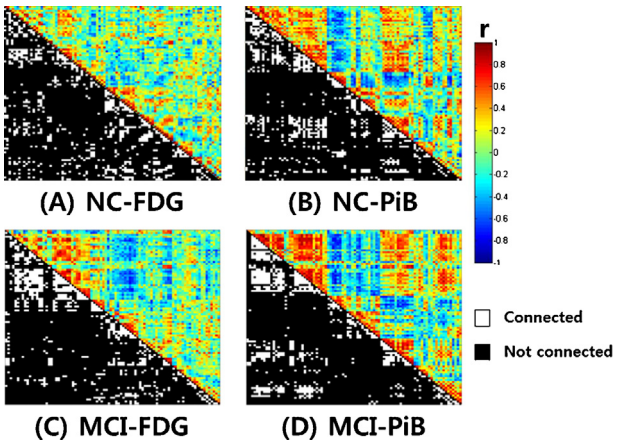

Fig. 1. Correlation matrices and the binarized matrices of NC and MCI groups. The first row shows the correlation matrices of (A) NC-FDG and (B) NC-PiB. The second row shows the correlation matrices of (C) MCI-FDG and (D) MCI-PiB. The upper triangular matrices show the weighted un-directed correlation matrices of each sub-group. The lower triangular matrices show the binarized matrices of the same sub-group at a sparsity level of 17%.

atlas was registered onto the standard space, we transferred the atlas ROI information onto the PET volume.

2.3. Network construction using graph theory

Whole brain connectivity was assessed using nodes and edges of a graph (Bullmore and Sporns, 2009; He and Evans, 2010). Nodes were assigned as 90 ROIs transferred from the atlas, which has also been used to assign nodes in previous studies (Hansen and Samuel, 1997; Tian et al., 2011; Wee et al., 2012; Seo et al., 2013; Wang et al., 2013; Hong et al., 2013; Varoquaux and Craddock, 2013). Each edge value was assumed to be the correlation value between two ROIs, which was entered into the correlation matrix as a matrix element. Correlation values were computed as a partial correlation, regressing out the effects of age and sex. We adopted a simple network model where un-directed and un-weighted edges were considered. The correlation matrix was converted into a binary matrix by a fixed density threshold method. The fixed density threshold ensures that the network graphs being compared have the same number of edges. We applied a wide range of density (between 6% and 40%), and compared correlation matrices of the different groups. Each group resulted in two correlation matrices, one from FDG-PET and the other from PiB-PET. A total of four correlation matrices were computed. Correlation matrices for each group together with the threshold matrices are shown in Fig. 1. The correlation matrices were further transformed using Fisher's *r*-to-*z* transform.

2.4. Combining correlation matrices

Given an imaging modality, one might compare two correlation matrices to assess differences between groups. If there are two matrices per group, one might take an element-wise average of matrices to arrive at a new correlation matrix and perform the ensuing connectivity analysis. In this way, certain patterns of correlation values in a matrix might be blurred. The average of a large correlation value and a small correlation value would be an intermediate value. We wanted to combine correlation values in a way analogous to logical AND and OR operations. The AND operation keeps a correlation value high only if two correlation values are high prior to a combining operation. In the same way, an AND operation keeps a correlation value low only if two correlation values are low before the combining operation. The OR operation keeps a correlation value high if one of two correlation values are high

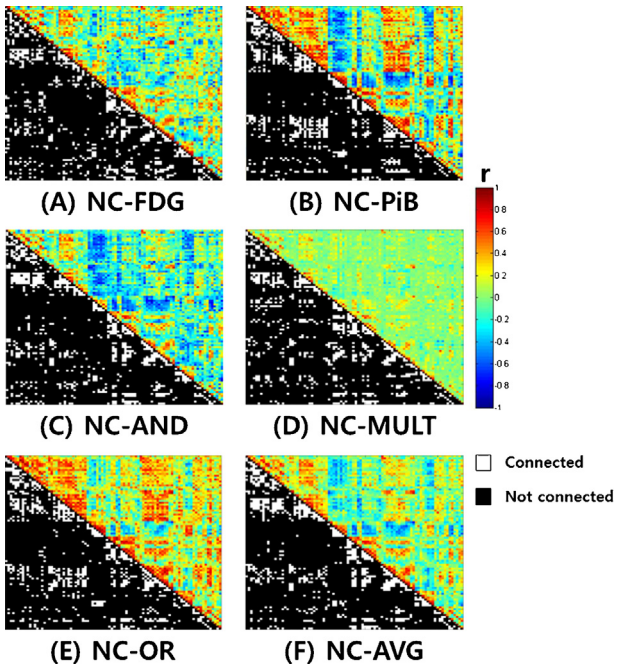

Fig. 2. Two correlation matrices, together with the results of combined correlation matrices, using various approaches for the NC group. The first row shows the correlation matrices of (A) NC-FDG and (B) NC-PiB. The second row shows the correlation matrices of (C) NC-AND and (D) NC-MULT. NC-MULT is the matrix obtained by element-wise multiplication. The third row shows the correlation matrices of (E) NC-OR and (F) NC-AVG. NC-AVG is the matrix obtained by the element-wise average.

prior to a combining operation. The AND operator of correlation matrices was implemented as an element-wise minimum operator. Using element-wise multiplication will lead to a similar combined-matrix value, but will negatively affect the combined value. In the specific case of data herein, if two correlation values were 0.3 (moderately low) and 0.7 (moderately high), we wanted to extract a value of 0.3 (moderately low) for the combined correlation value. Using element-wise multiplication results in a value of 0.21 (still moderately low), which is an approximate value. The OR operator of correlation matrices was implemented as an element-wise maximum operator. Using an element-wise average will lead to a similar combined-matrix value, but will negatively affect the combined value. Two correlation matrices of NC-FDG and NC-PiB, along with various approaches to combine the two matrices, are shown in Fig. 2.

2.5. Connectivity analysis

The correlation matrix of the brain network, whether combined or not, was further analyzed using connectivity analysis. We computed clustering coefficient (Cp) and characteristic path length (Lp) values to quantify properties of the network. The clustering coefficient reflects the average degree of local connectivity, while the characteristic path length reflects the functional integration of the entire network. The brain is considered a highly complex network, which can possess properties of both local specification and global integration. Many studies have reported that the brain network has a "small-world" property, which implies high values of local clustering (Cp) and similar path lengths (Lp) relative to matched random networks (Bullmore and Sporns, 2009; He and Evans, 2010; Watts and Strogatz, 1998). This "small-world" property reinforces findings that the brain is an efficient network, capable of local specification and global integration. We confirm the "small-world" property of the brain by comparing a given

network with a matched random network with the same node degree distribution. We generated 1000 random networks and then computed mean values of clustering coefficients and characteristic path lengths. Clustering coefficient and characteristic path length values were normalized by the respective mean values from the random network. The ratio of normalized clustering coefficients and characteristic path lengths is called the small-world index (σ = Cp_norm/Lp_norm). If a given network yields a small-world index with a value larger than 1, then the network is classified as a "small-world" network. We applied a wide range of sparsity, between 6% and 40% ($6\% \leq S \leq 40\%$, at 1% steps), and quantified small-world index values (Zhu et al., 2012). Betweenness centrality is another parameter to describe the brain network. Unlike the previous two parameters, betweenness centrality is a local parameter that quantifies the importance of a given node in terms of network organization. The betweenness centrality of a given node is the number of shortest paths between any two nodes that run through the given node, which quantifies how much information might go through the given node. In the analysis herein, the value of the betweenness centrality was normalized using the average value of betweenness centrality over the whole brain. If a given node has a normalized betweenness centrality value that is over 1.5, then the node is considered a hub node. Unlike the previous two network parameters, betweenness centrality is computed for each node, not for the entire network. Normalized betweenness centrality was computed at a sparsity level of 17%. This level of sparsity was chosen as the minimum sparsity at which all 90 ROIs are connected. All three brain network parameters – clustering coefficients, characteristic path lengths, and betweenness centrality – were computed using "brain connectivity analysis software" (http://www.brain-connectivity-toolbox.net) (Rubinov and Sporns, 2010).

2.6. Statistical tests

Four correlation matrices (FDG, PiB, AND, and OR) were obtained for each group. Group-wise differences based on the three network parameters (i.e., clustering coefficients, characteristic path lengths, and betweenness centrality) were assessed using non-parametric permutation tests. For each network parameter, 20 (or 15) participants were randomly assigned to the NC group, and the remaining participants were assigned to the MCI group. For the newly-assigned groups, the correlation matrices were computed for each group, and the three network parameters were subsequently computed. The process was repeated 7000 times, yielding a null distribution that would be used for group-wise differences. Significant differences between groups were assessed if group-wise differences resulted in a value outside the 95% interval of the null distribution (determined by two-tailed tests with $p < 0.05$). The non-parametric permutation test was repeated for the same sparsity range (between 6% and 40%) for clustering coefficients and characteristic path lengths. Correction for multiple comparisons was not adopted, because we were mainly interested in general trends of group-wise differences for the range of sparsity values. The same non-parametric tests were performed for the betweenness centrality at a sparsity level of 17%.

3. Results

3.1. Small-world property and group-wise differences

Networks constructed for both the NC and MCI groups demonstrated "small-world" characteristics for all four types of correlation matrices (FDG, PiB, AND, and OR), confirmed by small-world index values that were greater than 1 (Fig. 3). This shows that the brain is a "small-world" network in whichever ways that we construct the correlation matrices from two types of PET imaging.

Group-wise differences of cluster coefficients showed higher clustering coefficients in the MCI group relative to the NC group for the range of sparsity values (Fig. 4). This finding is consistent with previous research reporting increased clustering coefficients for MCI groups using FDG-PET (Seo et al., 2013; Daianu et al., 2013). Based on our analysis herein, using PiB-PET resulted in significant differences at more sparsity values. We observed significant differences at 14 sparsity values for PiB in comparison to significant differences at 11 sparsity values for FDG. PiB-PET is considered to have better sensitivity in detecting the progression of AD than FDG-PET (Mintun et al., 2006; Jack et al., 2008; Zhang et al., 2012). Thus, the increased sensitivity of PiB-PET might be translated to increased instances of significant differences at a wider range of sparsity values. Using the correlation matrix obtained by the AND operation resulted in significant differences at 13 sparsity values, while using the correlation matrix obtained by the OR operation resulted in significant differences at 18 sparsity values. One possible explanation for this finding is that the AND operation forces the combined correlation matrix to have a lower occurrence of high and low values in comparison to both the FDG correlation matrix and the PiB correlation matrix, thus leading to a lower chance of differences being found. Along the same lines, the OR operation forces the combined matrix to have a greater occurrence of high and low values, and thus leads to a greater chance of differences being found.

Group-wise differences of characteristic path lengths showed a higher characteristic path length in the NC group relative to the MCI group for a very limited range of sparsity values (Fig. 4). This finding is consistent with previous research reporting very few differences between MCI and NC groups using FDG-PET (Seo et al., 2013). According to our results, we observed significant differences at 2 sparsity values for PiB in comparison to significant differences at 1 sparsity value for FDG. Using the correlation matrix obtained by the AND operation resulted in significant differences at 7 sparsity values, while using the correlation matrix obtained by the OR operation resulted in no significant differences over the searched sparsity range. We observed significant differences at 7 sparsity values at the most, in comparison to significant differences at 18 sparsity values for clustering coefficients. Overall, using characteristic path lengths was not very sensitive in distinguishing between the MCI and NC groups. Using the correlation matrix by the AND operation resulted in significant differences at 7 sparsity values, in comparison to significant differences at 1 sparsity value in the case of FDG. One would expect to observe fewer differences by utilizing the AND operation, but we observed the opposite trend. Further discussion regarding this issue appears below.

3.2. AD progression and alteration of functional hubs

A hub node is a node whose betweenness centrality is higher than the betweenness centrality of nodes in the rest of the brain network. Thus a hub node is considered to be an important region in the brain. We assessed changes in the betweenness centrality of hub nodes in the MCI and NC groups. Hub nodes whose betweenness centrality decreased significantly ($p = 0.05$ level, one-tailed) between the NC and MCI groups were identified. We only searched for cases in which the MCI group had lower betweenness centrality in comparison to the betweenness centrality of the NC group, because the progression of AD is believed to negatively impact connections in many regions (He and Evans, 2010; Rubinov and Sporns, 2010; Tian et al., 2011; Zhu et al., 2012; Seo et al., 2013). Five regions were identified, as follows. The left anterior cingulum, right superior parietal, right fusiform, right inferior

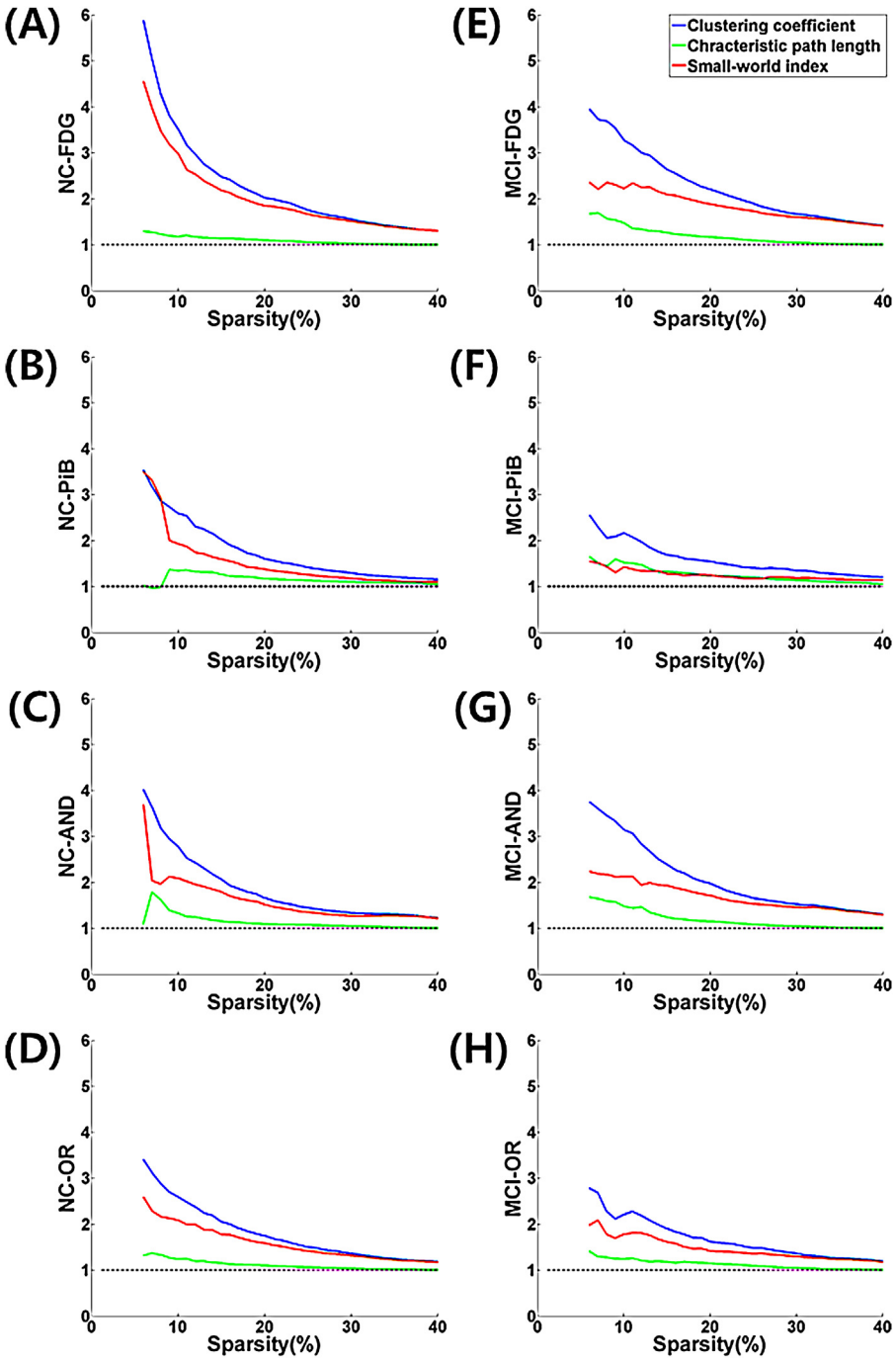

Fig. 3. Demonstration of the "small-world" property for the NC and MCI groups using various correlation matrices. The left column shows the "small-world" index values for (A) NC-FDG, (B) NC-PiB, (C) NC-AND, and (D) NC-OR. The right column shows the "small-world" index values for (E) MCI-FDG, (F) MCI-PiB, (G) MCI-AND, and (H) MCI-OR.

temporal gyrus, and right cuneus were found to have group-wise differences in betweenness centrality (Fig. 5 and Table 2). Previous studies have reported that these regions are differentially affected by the progression of AD (Koivunen et al., 2008; Förster et al., 2010; Ossenkoppele et al., 2012; Okamura et al., 2014). The left anterior cingulum was identified using FDG, PiB, and the OR correlation matrix. The regions showed significant changes for AD relative to normal in previous studies by Koivunen et al. (2008), Grimmer et al. (2009) and Mori et al. (2013). The region of the right superior parietal, reported about in studies by Edison et al. (2007), Devanand et al. (2010), Meyer et al. (2011) and Ossenkoppele et al. (2012), was identified using PiB and the OR correlation matrix. The region of the right fusiform, reported about in studies by Mosconi et al. (2010b), Förster et al. (2010), Bauer (2013) and Sanabria-Diaz et al. (2013), was identified using PiB and the AND correlation matrix. The region of the right inferior temporal gyrus, reported about in studies by Melrose et al. (2009), Mattsson et al. (2014) and Okamura et al. (2014), was identified using PiB and the AND correlation matrix. Finally, the region of the right cuneus, reported about in studies by Nestor et al. (2003), Förster et al. (2010), Tosun et al. (2011) and Codispoti et al. (2012), was identified using the OR and the AND correlation matrix. If we were limited to FDG-PET, then only the left anterior cingulum region could be identified. With the addition of PiB-PET and the AND/OR operations, we were able to locate four other ROIs related to AD progression in patients.

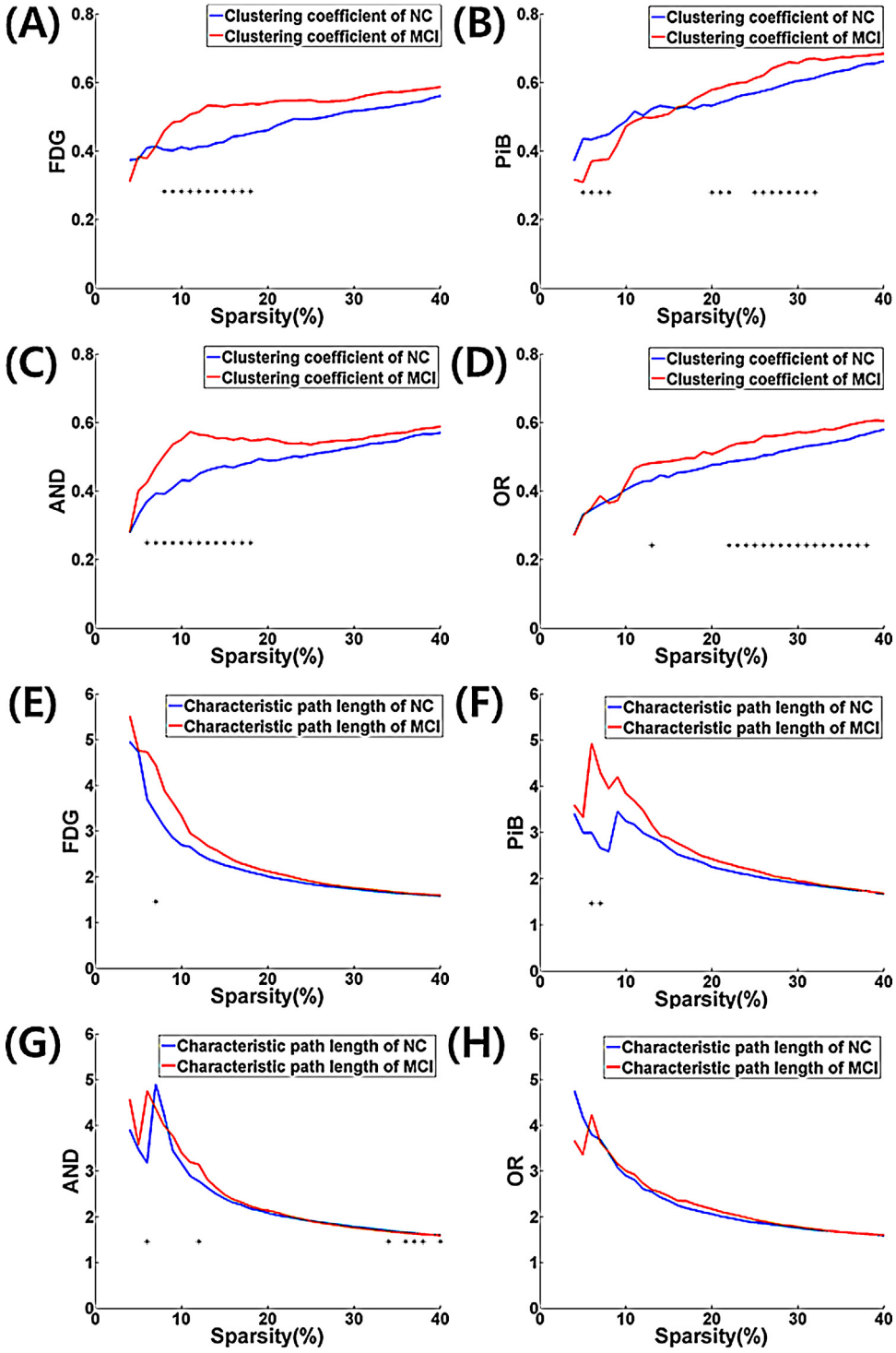

Fig. 4. Comparison of clustering coefficient and characteristic path length network parameters for the NC and MCI groups, based on various correlation matrices. Significant group-wise differences are noted with an asterisk (*). The first (top) and second row compare clustering coefficients from FDG, PiB, AND, and OR correlation matrices (A)–(D). The third and fourth (bottom) row compare characteristic path lengths from FDG, PiB, AND, and OR correlation matrices (E)–(H).

4. Discussion

This study is the first study to (1) perform connectivity analysis for both FDG-PET and PiB-PET, and (2) combine them using operations analogous to logical AND/OR operations. Our results found important regions differentially affected by the progression of AD. We focus on making distinctions between the MCI and NC groups so that our study might contribute to early detection of AD. Many existing studies consider only FDG-PET, but this study considers additional PiB-PET, a promising PET modality. Furthermore, we report findings based on combining the results of FDG-PET and PiB-PET imaging.

Our study selected 40 FDG-PET and 35 PiB-PET images from the ADNI database. Our findings showed five regions wherein significant changes in betweenness centrality were observed. Our findings failed to identify other regions, including the inferior

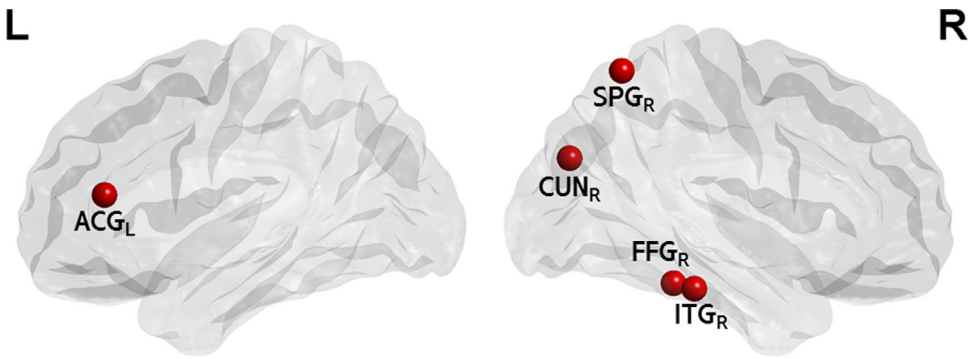

Fig. 5. Hub regions were visualized using the BrainNet Viewer (http://www.nitrc.org/projects/bnv/). The circle indicates the regions of a mild cognitive impairment (MCI) network, which show decreased betweenness centrality relative to the normal control (NC). L = left; R = right.

frontal gyrus, which are differentially affected by AD (Klunk et al., 2004; Miao et al., 2011; Seo et al., 2013). This may be due to the limited sample of the study. The ADNI database contained many more than 75 PET images, but once we applied criteria for separating the MCI group from the NC group and the image acquisition protocols, we were limited to 75 participants. A greater number of PET images could be obtained if we considered heterogeneous image acquisition protocols within a given group. In that case, however, the group-wise differences would be undesirably confounded by the difference in image acquisition.

The correlation matrices of PiB and FDG-PET were combined using element-wise minimum and maximum operations for AND and OR matrices. For clustering coefficients, our way of combing matrices worked well. Using the AND matrix led to observing differences at fewer sparsity values than individual PET (i.e., AND: 13 sparsity values; PiB: 14 sparsity values). Using the OR matrix led to observing differences at a greater number of sparsity values in comparison to individual PET (OR: 18 sparsity values; PiB: 14 sparsity values). The AND and OR matrices provided results in line with our expectations. We might go so far as to conjecture that FDG and PiB provide complementary information regarding clustering coefficients. For characteristic path lengths, using the AND matrix led to observing differences at a greater number of sparsity values in comparison to individual PET (AND: 7 sparsity values; PiB: 2 sparsity values), which was not expected. An explanation for this departure from expectation may be that PiB and FDG-PET provide contradictory information regarding characteristic path lengths.

Our connectivity analysis incorporated two different types of PET imaging. FDG-PET draws its contrast from region glucose uptake, which tends to be lower for MCI patients in comparison to NC patients. PiB-PET draws its contrast from beta-amyloid deposition, which tends to increase from NC to MCI patients. Our analysis was able to combine the results of these two types of imaging and find important regions for AD progression in terms of hub regions. The region of the right fusiform showed the greatest decrease in betweenness centrality (from 540 to 36) using PiB, which was the most significant difference among the five identified regions. This may imply that local deposition of beta-amyloid changes the most in that region, causing the disruption in connectivity parameters (Minoshima et al., 1997; Walsh and Selkoe, 2004; Buckner and Sepulcre, 2009). Another hub region associated with AD, the right cuneus, was identified using AND and OR correlation matrices (as opposed to PiB and FDG correlation matrices) (Nestor et al., 2003; Förster et al., 2010; Tosun et al., 2011; Codispoti et al., 2012). Similarly, the right superior parietal showed a decrease in betweenness centrality using PiB and OR correlation matrices. The right fusiform and right inferior temporal gyrus showed decreases in betweenness centrality using PiB and AND correlation matrices. These findings seem to imply that the combined AND or OR matrices provide additional information to complement PiB and FDG-PET images. Our results of FDG imaging showed a decrease in betweenness centrality for one region, the left anterior cingulum, while a previous study reports a decrease in betweenness centrality for both the left inferior frontal triangular and left precuneus (Seo et al., 2013). Our results of PiB imaging showed a decrease in betweenness centrality for three regions, including the right superior parietal, right fusiform, and right inferior temporal gyrus. These results might be in line with findings regarding the increased sensitivity of PiB for AD progression, considering that our use of PiB led to the identification of more affected regions (Zhang et al., 2012). Further studies with more data samples are needed to investigate this issue.

The connectivity analysis method adopted in this study was applied in FDG-PET studies to distinguish between normal and MCI patients (Seo et al., 2013). The identified regions showing

Table 2
ROIs showing significant decreases in betweenness centrality from NC to MCI groups.

ROI	Method adopted for the correlation matrix	Betweenness centrality value		*p*-Value
		NC	MCI	
Left anterior cingulum	FDG	186.86	96.76	<0.001
	PiB	367.52	77.07	<0.001
	OR	322.84	116.47	<0.001
Right superior parietal	PiB	253.39	145.58	<0.001
	OR	147.59	75.10	0.0298
Right fusiform	PiB	539.65	36.08	<0.001
	AND	206.59	80.68	<0.001
Right inferior temporal gyrus	PiB	392.00	269.10	0.0403
	AND	336.33	96.93	<0.001
Right cuneus	OR	133.60	11.17	<0.001
	AND	289.24	149.61	<0.001

significant group-wise difference were also reported in our study. We could not find studies using the same connectivity analysis for PiB-PET to distinguish between normal and MCI. A few studies involving PiB-PET and fMRI which bear some resemblance were found (Lim et al., 2014; Song et al., 2015). They used amyloid imaging to distinguish between comparison groups and performed fMRI connectivity analysis. Our study and the previous studies reported significant regions with group-wise difference, which are mostly consistent (Lim et al., 2014; Song et al., 2015). One study performed fMRI connectivity analysis to patients with positive and negative amyloid deposition and reported cingulate region as the significant region for group-wise difference (Lim et al., 2014). Another study also performed fMRI connectivity analysis to patients with positive and negative amyloid deposition determined by Florbetapir PET and reported the temporal lobe as the significant region (Song et al., 2015). The cingulate and temporal regions were included in the five identified regions of this study.

This study is cross-sectional study distinguishing between MCI and NC groups. One needs to collect longitudinal PET imaging and apply the connectivity analysis to the follow-up PET imaging to quantify progression of AD. One might perform connectivity analysis of the test patient's imaging and compare it with existing correlation matrices of NC or MCI groups. One possible way to achieve this task is to compare changes in correlation matrix before and after the addition of the test patient's data. For example, if the addition of the test patient's data resulted in small change in the NC correlation matrix but a large change in the MCI correlation matrix, one might treat this test patient's case as an MCI case. Another possibility is to construct the full correlation matrix based on single test patient imaging data using local morphological patterns (Wee et al., 2013). Then one might be able to compare test patient's correlation matrix with existing correlation matrices of NC and MCI group. This is left for future investigation.

We focused on well-known network parameters (i.e., clustering coefficients, characteristic path lengths, and betweenness centrality) to quantify the brain network. There are many promising network parameters, including degree centrality and eigenvector centrality, that may be better and more highly sensitive in making distinctions between patient brains in MCI and NC groups (De Haan et al., 2012; Binnewijzend et al., 2014).

We adopted a pre-defined atlas to transfer 90 ROIs to individual PET images. The atlas is based on structural parcellation of the entire brain. Other structural atlases divide the brain into more ROIs, namely 200 or 300 ROIs (Craddock et al., 2012; Varoquaux and Craddock, 2013). Using a more finely divided atlas may in fact provide better sensitivity in detecting changes related to the progression of AD. There are atlases derived from functional parcellation of the brain (Craddock et al., 2012; Varoquaux and Craddock, 2013). Using functional atlases may be a more sensitive method for locating specific regions related to functional changes in AD patients.

Acknowledgements

This study was supported in part by the Basic Science Research Program through grants of the National Research Foundation of Korea (grant numbers 2012R1A2A2A01005939, 20100023233, and 2013R1A2A2A04016262).

References

Anwander, A., Tittgemeyer, M., von Cramon, D.Y., Friederici, A.D., Knösche, T.R., 2007. Connectivity-based parcellation of Broca's Area. Cereb. Cortex 17, 816–825.

Berchtold, N.C., Cotman, C.W., 1998. Evolution in the conceptualization of Dementia and Alzheimer's disease: Greco-Roman period to the 1960. Neurobiol. Aging 19, 173–189.

Binnewijzend, M.A., Adriaanse, S.M., Van der Flier, W.M., Teunissen, C.E., de Munck, J.C., Stam, C.J., Scheltens, P., van Berckel, B.N.M., Barkhof, F., Wink, A.M., 2014. Brain network alterations in Alzheimer's disease measured by eigenvector centrality in fMRI are related to cognition and CSF biomarkers. Hum. Brain Mapp. 35, 2383–2393.

Bohnen, N., Djang, D., 2012. Effectiveness and safety of 18F-FDG PET in the evaluation of dementia: a review of the recent literature. J. Nucl. Med. 53, 59–71.

Braak, E., Griffing, K., Arai, K., Bohl, J., Bratzke, H., Braak, H., 1999. Neuropathology of Alzheimer's disease: what is new since A Alzheimer? Eur. Arch. Psychiatry Clin. Neurosci. 249 (Suppl.), 14–22.

Brookmeyer, R., 1998. Projections of Alzheimer's disease in the United States and the public health impact of delaying disease onset. Am. J. Public Health 88, 1337–1342.

Buckner, R., Sepulcre, J., 2009. Cortical hubs revealed by intrinsic functional connectivity: mapping, assessment of stability, and relation to Alzheimer's disease. J. Neurosci. 29, 1860–1873.

Bullmore, E., Sporns, O., 2009. Complex brain networks: graph theoretical analysis of structural and functional systems. Nat. Rev. Neurosci. 10, 186–198.

Carrillo, M.C., Bain, L.J., Frisoni, G.B., Weiner, M.W., 2012. Worldwide Alzheimer's disease neuroimaging initiative. Alzheimer's Dement. 8, 337–342.

Codispoti, K.-E.T., Beason-Held, L.L., Kraut, M.A., O'Brien, R.J., Rudow, G., Pletnikova, O., Crain, B., Troncoso, J.C., Resnick, S.M., 2012. Longitudinal brain activity changes in asymptomatic Alzheimer disease. Brain Behav. 2, 221–230.

Craddock, R.C., James, G.A., Holtzheimer, P.E., Hu, X.P., Mayberg, H.S., 2012. A whole brain fMRI atlas generated via spatially constrained spectral clustering. Hum. Brain Mapp. 33, 1914–1928.

Daianu, M., Jahanshad, N., Nir, T.M., Toga, A.W., Jack, C.R., Weiner, M.W., Thompson, P.M., 2013. Breakdown of brain connectivity between normal aging and Alzheimer's disease: a structural k-core network analysis. Brain Connect. 3, 407–422.

De Haan, W., van der Flier, W.M., Wang, H., Van Mieghem, P.F., Scheltens, P., Stam, C.J., 2012. Disruption of functional brain networks in Alzheimer's disease: what can we learn from graph spectral analysis of resting-state magnetoencephalography? Brain Connect. 2, 45–55.

Devanand, D.P., Mikhno, A., Pelton, G.H., Cuasay, K., Pradhaban, G., Dileep Kumar, J.S., Upton, N., Lai, R., Gunn, R.N., Libri, V., Liu, X., van Heertum, R., Mann, J.J., Parsey, R.V., 2010. Pittsburgh compound B (11C-PIB) and fluorodeoxyglucose (18 F-FDG) PET in patients with Alzheimer disease, mild cognitive impairment, and healthy controls. J. Geriatr. Psychiatry Neurol. 23, 185–198.

Edison, P., Archer, H., Hinz, R., Hammers, A., 2007. Amyloid, hypometabolism, and cognition in Alzheimer disease. An PIB and FDG PET study. Neurology 68, 501–508.

Folstein, M., Folstein, S., McHugh, P., 1975. Mini-mental state: a practical method for grading the cognitive state of patients for the clinician. J. Psychiatr. Res. 12, 189–198.

Förster, S., Teipel, S., Zach, C., Rominger, A., Cumming, P., La Fougere, C., Yakushev, I., Haslbeck, M., Hampel, H., Bartenstein, P., Bürger, K., 2010. FDG-PET mapping the brain substrates of visuo-constructive processing in Alzheimer's disease. J. Psychiatr. Res. 44, 462–469.

Foster, N.L., Heidebrink, J.L., Clark, C.M., Jagust, W.J., Arnold, S.E., Barbas, N.R., DeCarli, C.S., Turner, R.S., Koeppe, R.A., Higdon, R., Minoshima, S., 2007. FDG-PET improves accuracy in distinguishing frontotemporal dementia and Alzheimer's disease. Brain 130, 2616–2635.

Fripp, J., Bourgeat, P., Acosta, O., Raniga, P., Modat, M., Pike, K.E., Jones, G., O'Keefe, G., Masters, C.L., Ames, D., Ellis, K.A., Maruff, P., Currie, J., Villemagne, V.L., Rowe, C.C., Salvado, O., Ourselin, S., 2008. Appearance modeling of 11C PiB PET images: characterizing amyloid deposition in Alzheimer's disease, mild cognitive impairment and healthy aging. Neuroimage 43, 430–439.

Frisoni, G., Fox, N., Jack, C., 2010. The clinical use of structural MRI in Alzheimer disease. Nat. Rev. Neurol. 6, 67–77.

Friston, K., Holmes, A., 1994. Statistical parametric maps in functional imaging: a general linear approach. Hum. Brain Mapp. 2, 189–210.

Greicius, M.D., Srivastava, G., Reiss, A.L., Menon, V., 2004. Default-mode network activity distinguishes Alzheimer's disease from healthy aging: evidence from functional MRI. Proc. Natl. Acad. Sci. U.S.A. 101, 4637–4642.

Grimmer, T., Henriksen, G., Wester, H.-J., Förstl, H., Klunk, W.E., Mathis, C.A., Kurz, A., Drzezga, A., 2009. Clinical severity of Alzheimer's disease is associated with PIB uptake in PET. Neurobiol. Aging 30, 1902–1909.

Hansen, L.A., Samuel, W., 1997. Criteria for Alzheimer's disease and the nosology of dementia with Lewy bodies. Neurology 48, 126–132.

Hatashita, S., Yamasaki, H., 2013. Diagnosed mild cognitive impairment due to Alzheimer's disease with PET biomarkers of beta amyloid and neuronal dysfunction. PLOS ONE 8, e66877.

He, Y., Chen, Z.J., Evans, A.C., 2007. Small-world anatomical networks in the human brain revealed by cortical thickness from MRI. Cereb. Cortex 17, 2407–2419.

He, Y., Evans, A., 2010. Graph theoretical modeling of brain connectivity. Curr. Opin. Neurol. 23, 341–350.

Hebert, L., Scherr, P., 2003. Alzheimer disease in the US population: prevalence estimates using the 2000 census. Arch. Neurol. 60, 1119–1122.

Hong, S.-B., Zalesky, A., Cocchi, L., Fornito, A., Choi, E.-J., Kim, H.-H., Suh, J.-E., Kim, C.-D., Kim, J.-W., Yi, S.-H., 2013. Decreased functional brain connectivity in adolescents with internet addiction. PLOS ONE 8, e57831.

Ishii, K., 2013. PET approaches for diagnosis of dementia. Am. J. Neuroradiol. (Epub ahead of print).

Jack, C.R., Lowe, V.J., Senjem, M.L., Weigand, S.D., Kemp, B.J., Shiung, M.M., Knopman, D.S., Boeve, B.F., Klunk, W.E., Mathis, C.A., Petersen, R.C., 2008. 11C PiB and

structural MRI provide complementary information in imaging of Alzheimer's disease and amnestic mild cognitive impairment. Brain 131, 665–680.
Jenkinson, M., Beckmann, C.F., Behrens, T.E.J., Woolrich, M.W., Smith, S.M., 2012. FSL. Neuroimage 62, 782–790.
Klunk, W., Engler, H., Nordberg, A., 2004. Imaging brain amyloid in Alzheimer's disease with Pittsburgh compound-B. Ann. Neurol. 55, 306–319.
Koivunen, J., Verkkoniemi, A., Aalto, S., Paetau, A., Ahonen, J.-P., Viitanen, M., Någren, K., Rokka, J., Haaparanta, M., Kalimo, H., Rinne, J.O., 2008. PET amyloid ligand [11C]PIB uptake shows predominantly striatal increase in variant Alzheimer's disease. Brain 131, 1845–1853.
Lee, D.Y., Fletcher, E., Martinez, O., Ortega, M., Zozulya, N., Kim, J., Tran, J., Buonocore, M., Carmichael, O., DeCarli, C., 2009. Regional pattern of white matter microstructural changes in normal aging, MCI, and AD. Neurology 73, 1722–1728.
Lim, H.K., Nebes, R., Snitz, B., Cohen, A., Mathis, C., Price, J., Weissfeld, L., Klunk, W., Aizenstein, H.J., 2014. Regional amyloid burden and intrinsic connectivity networks in cognitively normal elderly subjects. Brain 137, 3327–3338.
Bauer, M.C., 2013. Differentiating between Normal aging mild cognitive impairment, and Alzheimer's disease with FDG-PET: effects of normalization region and partial volume correction method. J. Alzheimer's Dis. Park. 3, 1–9.
Matsuda, H., 2007. Role of neuroimaging in Alzheimer's disease, with emphasis on brain perfusion SPECT. J. Nucl. Med. 48, 1289–1300.
Mattsson, N., Tosun, D., Insel, P.S., Simonson, A., Jack, C.R., Beckett, L.A., Donohue, M., Jagust, W., Schuff, N., Weiner, M.W., 2014. Association of brain amyloid-β with cerebral perfusion and structure in Alzheimer's disease and mild cognitive impairment. Brain 137, 1550–1561.
Melrose, R.J., Campa, O.M., Harwood, D.G., Osato, S., Mandelkern, M.A., Sultzer, D.L., 2009. The neural correlates of naming and fluency deficits in Alzheimer's disease: an FDG-PET study. Int. J. Geriatr. Psychiatry 24, 885–893.
Meyer, C., Boes, J., Kim, B., Bland, P., 1997. Demonstration of accuracy and clinical versatility of mutual information for automatic multimodality image fusion using affine and thin-plate spline warped geometric. Med. Image Anal. 1, 195–206.
Meyer, P.T., Hellwig, S., Amtage, F., Rottenburger, C., Sahm, U., Reuland, P., Weber, W.A., Hüll, M., 2011. Dual-biomarker imaging of regional cerebral amyloid load and neuronal activity in dementia with PET and 11C-labeled Pittsburgh compound B. J. Nucl. Med. 52, 393–400.
Miao, X., Wu, X., Li, R., Chen, K., Yao, L., 2011. Altered connectivity pattern of hubs in default-mode network with Alzheimer's disease: an Granger causality modeling approach. PLoS One 6, e25546.
Minoshima, S., Giordani, B., Berent, S., 1997. Metabolic reduction in the posterior cingulate cortex in very early Alzheimer's disease. Ann. Neurol. 42, 85–94.
Mintun, M.A., Larossa, G.N., Sheline, Y.I., Dence, C.S., Lee, S.Y., Mach, R.H., Klunk, W.E., Mathis, C.A., DeKosky, S.T., Morris, J.C., 2006. [11C]PIB in a nondemented population: potential antecedent marker of Alzheimer disease. Neurology 67, 446–452.
Mori, T., Shimada, H., Shinotoh, H., 2013. Amyloid, hypometabolism, and cognition in Alzheimer disease: an [11C]PIB and [18F]FDG PET study. Neurology 85, 449–455.
Morris, J., 1993. The Clinical Dementia Rating (CDR): current version and scoring rules. Neurology 43, 2412–2414.
Mosconi, L., Berti, V., Glodzik, L., 2010a. Pre-clinical detection of Alzheimer's disease using FDG-PET, with or without amyloid imaging. J. Alzheimer's Dis. 20, 843–854.
Mosconi, L., Rinne, J.O., Tsui, W.H., Berti, V., Li, Y., Wang, H., Murray, J., Scheinin, N., Någren, K., Williams, S., Glodzik, L., De Santi, S., Vallabhajosula, S., de Leon, M.J., 2010b. Increased fibrillar amyloid-{beta} burden in normal individuals with a family history of late-onset Alzheimer's. Proc. Natl. Acad. Sci. U.S.A. 107, 5949–5954.
Nestor, P., Caine, D., Fryer, T., 2003. The topography of metabolic deficits in posterior cortical atrophy (the visual variant of Alzheimer's disease) with FDG-PET. J. Neurol. Neurosurg. Psychiatry 74, 1521–1529.
Okamura, N., Furumoto, S., Fodero-Tavoletti, M.T., Mulligan, R.S., Harada, R., Yates, P., Pejoska, S., Kudo, Y., Masters, C.L., Yanai, K., Rowe, C.C., Villemagne, V.L., 2014. Non-invasive assessment of Alzheimer's disease neurofibrillary pathology using 18F-THK5105 PET. Brain 137, 1762–1771.
Ossenkoppele, R., Zwan, M.D., Tolboom, N., van Assema, D.M.E., Adriaanse, S.F., Kloet, R.W., Boellaard, R., Windhorst, A.D., Barkhof, F., Lammertsma, A.A., Scheltens, P., van der Flier, W.M., van Berckel, B.N.M., 2012. Amyloid burden and metabolic function in early-onset Alzheimer's disease: parietal lobe involvement. Brain 135, 2115–2125.
Rubinov, M., Sporns, O., 2010. Complex network measures of brain connectivity: uses and interpretations. Neuroimage 52, 1059–1069.
Sanabria-Diaz, G., Martínez-Montes, E., Melie-Garcia, L., 2013. Glucose metabolism during resting state reveals abnormal brain networks organization in the Alzheimer's disease and mild cognitive impairment. PLOS ONE 8, e68860.
Seo, E., Lee, D., Lee, J., Park, J., Sohn, B., 2013. Whole-brain functional networks in cognitively normal, mild cognitive impairment, and Alzheimer's disease. PLOS ONE 8, e53922.
Song, Z., Insel, P.S., Buckley, S., Yohannes, S., Mezher, A., Simonson, A., Wilkins, S., Tosun, D., Mueller, S., Kramer, J.H., Miller, B.L., Weiner, X.W., 2015. Brain amyloid-β burden is associated with disruption of intrinsic functional connectivity within the medial temporal lobe in cognitively normal elderly. J. Neurosci. 35, 3240–3247.
Tian, L., Wang, J., Yan, C., He, Y., 2011. Hemisphere- and gender-related differences in small-world brain networks: a resting-state functional MRI study. Neuroimage 54, 191–202.
Tosun, D., Schuff, N., Mathis, C.A., Jagust, W., Weiner, M.W., 2011. Spatial patterns of brain amyloid-beta burden and atrophy rate associations in mild cognitive impairment. Brain 134, 1077–1088.
Tzourio-Mazoyer, N., Landeau, B., Papathanassiou, D., Crivello, F., Etard, O., Delcroix, N., Mazoyer, B., Joliot, M., 2002. Automated anatomical labeling of activations in SPM using a macroscopic anatomical parcellation of the MNI MRI single-subject brain. Neuroimage 15, 273–289.
Varoquaux, G., Craddock, R.C., 2013. Learning and comparing functional connectomes across subjects. Neuroimage 80, 405–415.
Walsh, D., Selkoe, D., 2004. Deciphering the molecular basis of memory failure in Alzheimer's disease. Neuron 44, 181–193.
Wang, J., Zuo, X., Dai, Z., Xia, M., Zhao, Z., Zhao, X., 2013. Disrupted functional brain connectome in individuals at risk for Alzheimer's disease. Biol. Psychiatry 73, 472–481.
Watts, D., Strogatz, S., 1998. Collective dynamics of small-world networks. Nature 393, 440–442.
Wee, C.Y., Yap, P.T., Shen, D., 2013. Prediction of Alzheimer's disease and mild cognitive impairment using cortical morphological patterns. Hum. Brain Mapp. 34, 3411–3425.
Wee, C.-Y., Yap, P.-T., Zhang, D., Denny, K., Browndyke, J.N., Potter, G.G., Welsh-Bohmer, K.A., Wang, L., Shen, D., 2012. Identification of MCI individuals using structural and functional connectivity networks. Neuroimage 59, 2045–2056.
Wheeler, A.L., Wessa, M., Szeszko, P.R., Foussias, G., Chakravarty, M.M., Lerch, J.P., DeRosse, P., Remington, G., Mulsant, B.H., Linke, J., Malhotra, A.K., Voineskos, A.N., 2015. Further neuroimaging evidence for the deficit subtype of Schizophrenia. JAMA Psychiatry, E1–E10.
Zalesky, A., Fornito, A., Bullmore, E., 2012. On the use of correlation as a measure of network connectivity. Neuroimage 60, 2096–2106.
Zhang, S., Han, D., Tan, X., Feng, J., Guo, Y., Ding, Y., 2012. Diagnostic accuracy of 18 F-FDG and 11 C-PIB-PET for prediction of short-term conversion to Alzheimer's disease in subjects with mild cognitive impairment. Int. J. Clin. Pract. 66, 185–198.
Zhu, W., Wen, W., He, Y., Xia, A., Anstey, K.J., Sachdev, P., 2012. Changing topological patterns in normal aging using large-scale structural networks. Neurobiol. Aging 33, 899–913.